

Learning Rolling Shutter Correction from Real Data without Camera Motion Assumption

Jiawei Mo¹, Md Jahidul Islam², Junaed Sattar³ *†

Abstract

The rolling shutter mechanism in modern cameras generates distortions as the images are formed on the sensor through a row-by-row read-out process; this is highly undesirable for photography and vision-based algorithms (*e.g.*, structure-from-motion and visual SLAM). In this paper, we propose a deep neural network to predict depth and camera poses for single-frame rolling shutter correction. Compared to the state-of-the-art, the proposed method has no assumptions on camera motion. It is enabled by training on real images captured by rolling shutter cameras instead of synthetic ones generated with certain motion assumption. Consequently, the proposed method performs better for real rolling shutter images. This makes it possible for numerous vision-based algorithms to use imagery captured using rolling shutter cameras and produce highly accurate results. Our evaluations on the TUM rolling shutter dataset using DSO and COLMAP validate the accuracy and robustness of the proposed method.

1 Introduction

Computer vision has been one of the most commonly-used sensing modalities in robotics, empowered by the low cost, low power consumption of camera sensors, and the rich information they provide. For the underlying image read-out mechanism, cameras either use a global shutter or rolling shutter system. Most CCD (Charge-Coupled Device) cameras use global shutters, while most CMOS (Complementary Metal–Oxide–Semiconductor) cameras employ rolling shutters. While global shutter cameras capture the entire image at once, the rolling shutter cameras capture the image row by row. As the camera can move arbitrarily during its exposure, the pixels on different rows end up having different optical centers for rolling shutter cameras. Most vision algorithms are

*The authors are with the Department of Computer Science and Engineering (CSE), Minnesota Robotics Institute (MnRI), University of Minnesota Twin Cities, Minneapolis, MN, USA. Email: {¹moxxx066, ²islam034, ³junaed}@umn.edu.

†*This work was supported by the US National Science Foundation Award IIS #1637875, the University of Minnesota Doctoral Dissertation Fellowship, and the MnRI Seed Grant.

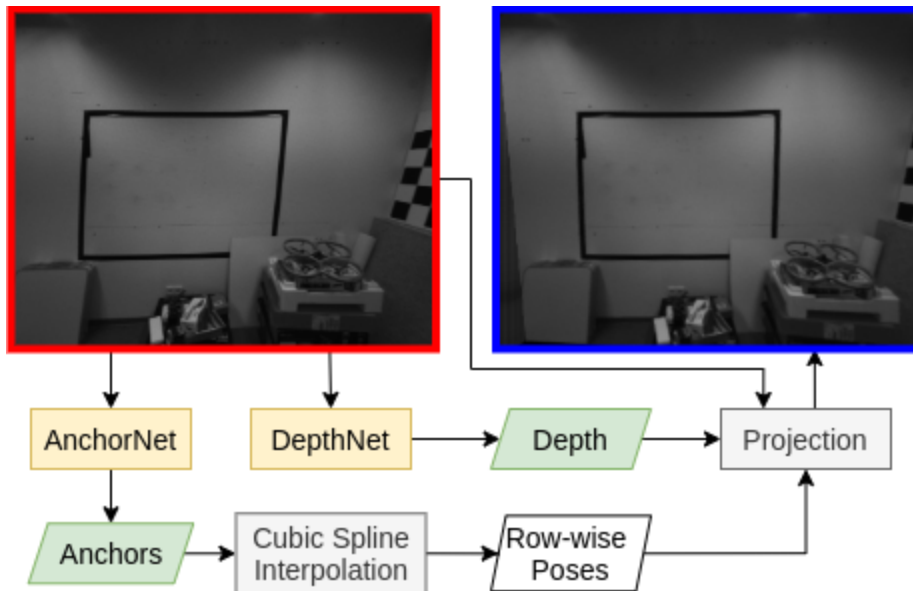


Figure 1: An overview of the proposed system: given an RS image, the pixel-wise depth is generated by DepthNet, whereas the AnchorNet predicts a set of pose anchors that are interpolated for a row-wise camera pose estimation. These pose estimates and depth maps are subsequently used for geometric projection to recover the corresponding GS image. [Red: input RS image; Yellow: deep neural networks; Green: network outputs; Blue: recovered GS image]

incapable of accounting for the distortions of rolling shutter cameras, and consequently perform poorly with those. However, most consumer-grade cameras are rolling shutter (*e.g.*, smartphone cameras), which creates a challenge in making vision-based computing more ubiquitous.

Computer vision algorithms can be tuned for rolling shutter cameras (*e.g.*, [1], [22], [8]), but the adaptation process is non-trivial. Constant velocity assumption is made in [22] to model the camera motion. In [8], IMU poses are used to interpolate a pose for each image feature. Alternatively, the rolling shutter images can be rectified before routing into the vision algorithms. Such rolling shutter correction algorithms can be categorized into multi-view methods [19, 29] and single-view methods [10, 17]. Traditionally, multi-view methods explore the relative geometry between images for rolling shutter correction, while the single-view methods rely on specific features (*e.g.*, straight lines in [17]) due to the lack of geometric information.

With the emergence of deep learning [6], numerous neural network-based models have been proposed to learn geometric information from images for problems such as single-image depth estimation [3, 2] and inferring structure-from-motion [27, 26]. In recent years, several research works have addressed the problem of ‘automatic rolling shutter correction’ as well and have reported

inspiring results [18, 30]. Due to the ill-posed nature of the problem, existing methods adopt simplified formulations by making various assumptions on the camera motion in their data generation and learning processes. For instance, Zhuang *et al.* [30] synthesize rolling shutter images from global shutter images under the assumption of a constant velocity in camera motion. Hence, their deep networks are trained and tested on synthetic data generated by emulating only a restricted set of camera motions. Moreover, Rengarajan *et al.* [18] assume only 2-degree-of-freedom camera motions while handling rolling shutter distortions. However, in many real-life applications, particularly for mobile robots in field environments, such assumptions are not realistic and are often invalid.

In this paper, we propose a novel approach to train a deep neural network for correcting image distortions arising from a rolling shutter mechanism without making any assumptions on the camera motion. We utilize the TUM rolling shutter dataset [22] for data generation; we first estimate the depth of each pixel in a rolling shutter (**RS**) image and recover its row-wise camera poses, which we subsequently use to reconstruct the corresponding global shutter (**GS**) image. This two-step process is analogous to the one by Zhuang *et al.* [30], who proposed DepthNet and VelocityNet for the depth estimation and camera pose estimation, respectively. However, VelocityNet incorporates a *constant velocity* assumption on camera motion which is not always valid in natural RS images. We address this issue by proposing **AnchorNet**, which learns a set of *pose anchors* (see Fig. 1) for row-wise camera pose estimation that eliminates the strong motion assumptions of VelocityNet. In fact, we demonstrate that the VelocityNet is the base case of AnchorNet (*i.e.*, when a single anchor is considered). Hence, it offers significantly more learning capacity for deep rolling shutter correction. An overview of our proposed system is illustrated in Fig. 1. In summary, the contributions of this work are three-fold: (*i*) a novel approach to generate RS/GS image pairs with no camera motion assumption, (*ii*) a robust deep visual model named AnchorNet that learns to correct rolling shutter distortion without camera motion assumptions, and (*iii*) extensive experimental validations of AnchorNet and the proposed data generation approach for rolling shutter correction.

Such an assumption-free mechanism to correct rolling shutter distortions is immensely useful in numerous robotic applications as it enables the use of imaging sensors regardless of their shutter mechanisms. Our experiments suggest that the proposed system achieves superior accuracy and robustness compared to the state-of-the-art methods, especially with arbitrary camera motions (see Sec. 4). Our implementation and dataset are available at <https://github.com/IRVLab/unrolling>.

2 Related Work

Removing RS distortions from images has several benefits as discussed in the previous sections, and finds utility in computer vision, robotics, consumer mobile photography, and a number of other applications. Several neural networks have

been proposed recently addressing this problem of single-frame rolling shutter correction. For example, Rengarajan *et al.* [18] proposed a convolutional neural network (CNN) architecture to predict the camera motion during exposure. The predicted motions are up-sampled using a polynomial function to get row-wise components of camera motion, which is subsequently used to correct the rolling shutter distortion. This approach is feasible because the camera motion is limited to two dimensions (*i.e.*, x -axis translation and z -axis rotation). The mapping function relating the coordinates of the RS pixel to its undistorted correspondence is fully determined by this 2D motion.

The work by Zhuang *et al.* [30] eliminates the 2D motion assumption above and enables full (6D) camera motion. They proposed VelocityNet to predict the camera velocity during exposure. The camera pose for each image row is calculated by the predicted velocity with the constant velocity assumption. Meanwhile, they adapt DispNet [14] (referred to as DepthNet) to predict pixel-wise depth in the RS image. With the camera pose and the depth, the undistorted GS image is generated by projection. In this work, we further eliminate the constant velocity assumption by extending their VelocityNet to our AnchorNet, which predicts multiple anchors for pose interpolation. The anchor interpolation idea is partially inspired by [18].

Data is essential for training neural networks. To train neural networks for rolling shutter correction, a large set of GS/RS image pairs is needed. However, to the best of our knowledge, there is no publicly available dataset specifically for training or benchmarking rolling shutter correction methods. The authors of [18] generate RS images from GS image datasets. For each GS image, they generate a random 2D camera motion and construct a mapping function to get the corresponding RS image. Subsequently, they train a CNN to perform the inverse action. Zhuang *et al.* [30], in the same vein, use a GS image dataset [5] to generate RS images. For each GS image pair, they run stereo matching to get a depth map; with a randomly-generated 6D camera velocity, they render an RS image under the constant camera velocity assumption. However, these two approaches cannot fully capture the real rolling shutter distortion due to their strong camera motion assumptions (see Sec. 4).

The TUM rolling shutter dataset [22] has been proposed to benchmark visual-inertial SLAM with rolling shutter cameras, captured by the device shown in Fig. 2. The device is equipped with a pair of synchronized RS/GS cameras, an IMU, and a motion capture system recording ground truth poses. We use this dataset to generate RS/GS image pairs without motion assumption.

3 Methodology

3.1 Dataset Generation

Our training data is generated from the TUM rolling shutter dataset [22]. To the best of our knowledge, it is the only publicly available dataset with synchronized RS/GS image pairs and camera poses. The RS/GS images are captured at 20Hz

with 1280×1024 resolution; we mark the GS camera as **cam₀** and the RS camera as **cam₁** (see Fig. 2). The ground truth pose is recorded by a motion capture system running at 120Hz. The time difference between two consecutive rows in an RS image is approximately $29.4737\mu s$. Additionally, IMU data at 200Hz is also provided but not used here. We refer interested readers to [22] for more details on this dataset.

The RS images captured by **cam₁** are used as inputs to our neural network. However, we cannot directly use the GS images as ground truth because they are captured by another camera. Hence, we recover the GS images at the location of **cam₁**. For clarity, we mark the GS images captured from **cam₀** as **GS₀** images and the recovered GS images as **GS₁**. As seen in Fig. 2, the idea is to recover a depth map from the stereo configuration and project points to the pose of the first image row of **cam₁** to get the **GS₁** images.

Recovering depth from a **GS₀** image and corresponding RS image is more challenging than from a pair of GS images. The rolling shutter distortion breaks the stereo epipolar constraint; even after stereo rectification, the pixel correspondences are not necessarily located in the same row, which makes conventional stereo matching algorithms (*e.g.*, [11]) inapplicable. Hence, we abandon the stereo constraint and adopt PWC-Net [25], the state-of-the-art optical flow algorithm, to find the optical flow between the **GS₀**/**RS** image pairs. For robustness, we filter the correspondences by standard bi-directional matching.

In addition to the pixel correspondence, the relative camera pose is also required for depth recovery. The rolling shutter mechanism makes the camera pose no longer consistent for all pixels in the RS image. Thus, row-wise camera poses are required. Unfortunately, the motion capture system is not efficient enough to capture a pose for every image row, even after we downsize the image resolution to 320×256 in this project. Since the motion capture system runs at 120Hz, the time interval between two poses is $8333.3\mu s$; the time to read out the entire RS image is $(1024 - 1) \times 29.4737\mu s = 30151.6\mu s$. As a result, we have about 3.6 poses for all 256 rows in the RS image, which is too sparse. To solve this problem, we adopt cubic spline interpolation [20] on the sparse poses to get a smooth pose for each row in the RS image. Since lens distortion is corrected

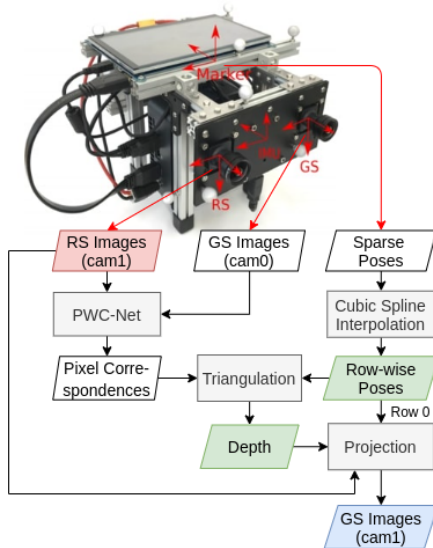


Figure 2: The data capture device used in [22] and an overview of the image processing pipeline. [Red: input RS image; Green: ground truth; Blue: recovered GS image]

during image preprocessing, we maintain a distortion lookup table to find the original scan-line when querying the pose for each pixel.

With the pixel correspondence (p_{GS_0}, p_{RS}) from PWC-Net and the row-wise camera pose $T_{p_{RS}}^{GS_0}$ from cubic spline interpolation, we get the depth map d_{RS} and corresponding 3D points X_{RS} by solving the following triangulation problem:

$$d_{RS} \begin{bmatrix} p_{RS} \\ 1 \end{bmatrix} = K_{RS} X_{RS}, \quad (1)$$

$$d_{GS_0} \begin{bmatrix} p_{GS_0} \\ 1 \end{bmatrix} = K_{GS_0} T_{p_{RS}}^{GS_0} \begin{bmatrix} X_{RS} \\ 1 \end{bmatrix}. \quad (2)$$

Here, K_{RS} and K_{GS_0} are known camera intrinsic parameters. The depth filter [28] is also used for further refinements; however, the improvement margins were insignificant and hence it is omitted in our final implementation.

Finally, we recover the pixels p_{GS_1} in GS_1 image by projecting the 3D points X_{RS} to the pose of the first row in RS frame (*i.e.*, $T_{p_{RS}}^{GS_1} = T_{p_{RS}}^{RS_{row0}}$) as

$$d_{GS_1} \begin{bmatrix} p_{GS_1} \\ 1 \end{bmatrix} = K_{RS} T_{p_{RS}}^{GS_1} \begin{bmatrix} X_{RS} \\ 1 \end{bmatrix}. \quad (3)$$

3.2 AnchorNet Architecture

As mentioned earlier, our end-to-end pipeline for learning rolling shutter correction is inspired by Zhuang *et al.* [30]. They proposed DepthNet for single-image depth estimation and VelocityNet for the row-wise camera pose estimation. The output of VelocityNet is a 6D vector representing camera velocity, which is multiplied by the relative readout time to get row-wise camera poses by assuming that the camera velocity is constant during exposure. We relax this motion assumption by learning to regress N pose anchors in the proposed AnchorNet model.

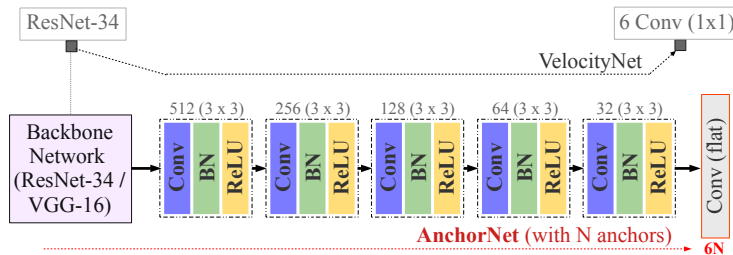


Figure 3: The network architecture of AnchorNet; a backbone feature extraction network (ResNet-34 or VGG-16) is followed by five convolutional blocks that learn $6N$ parameters where N denotes the number of anchors. Notice that it reduces to VelocityNet [30] with the default choice of a ResNet-34 backbone and $N = 1$ anchor.

To validate this conceptual design to eliminate the motion assumption, we incorporate minimal changes to our learning pipeline. Specifically, we keep the DepthNet unchanged, which adapts the DispNet [14] for depth estimation. Moreover, we adopt a holistic network architecture for AnchorNet which can be reduced to VelocityNet as the base case.

The detailed architecture of AnchorNet is illustrated in Fig. 3. We use the standard ResNet-34 network [9] for hierarchical feature extraction; we also provide the option of using a VGG-16 [23] backbone as well. The extracted low dimensional features are further exploited by five sequential convolutional blocks, each of which consists of a convolutional (**Conv**) layer, followed by batch normalization (**BN**) [12] and rectified linear unit (**ReLU**) activation [16]. Given a pre-specified number of anchors N , the output layer regresses $6N$ numbers, *i.e.*, 6D vector for each *pose anchor*. With the first image row being identity pose anchor, a cubic spline is reconstructed from the anchors to subsequently get a pose for each image row. Here, we identify two special cases:

- When $N = 1$, AnchorNet degenerates to the VelocityNet with only 6D output, essentially enforcing the constant velocity assumption.
- When $N = \text{image height}$, AnchorNet directly predicts poses for every image row, hence the cubic interpolation is no longer needed.

We studied other cases as well by varying the number of anchors in between. We empirically find that having more anchors enables the spline to represent more complex camera motion. We present the ablation results and other experimental validations in the next section.

4 Experimental Evaluation

By applying the data generation process described in Sec. 3.1 on the TUM rolling shutter dataset [22], we get 9495 RS images with corresponding depth maps and row-wise camera poses. This number is slightly less than the total number of frames (9523) in the dataset because some frames at the beginning or end of a few sequences were not recorded by the motion capture system, hence they were discarded. We utilize the remaining 9495 frames to generate training pairs for the supervised learning of rolling shutter correction without any camera motion assumptions.

In the evaluation, we quantify rolling shutter distortion by the standard end-point error (EPE) metric which measures the average Euclidean distance between the distorted and undistorted pixels. It is defined as follows

$$EPE(I) = \frac{1}{|I|} \sum_{p \in I} \|p - p_{GS_1}(p)\|_2.$$

Here, $|I|$ is the number of pixels in a given query image I , while $p_{GS_1}(p)$ is the corresponding pixel in GS_1 (ground truth image) for every pixel $p \in I$.

Table 1: EPE and DSO ATE with an increasing number of anchors; the results are based on the ground truth for sequence #2 in the TUM dataset.

Anchor	1	2	4	8	16	32	64	128	256
EPE (px)	0.312	0.236	0.189	0.179	0.179	0.180	0.180	0.180	0.180
ATE (m)	0.157	-	-	0.151	-	-	-	-	-

4.1 Generated Data Verification

Since the EPE is evaluated w.r.t. the GS_1 images generated by our proposed method, we need to verify the validity of GS_1 images. To do so, we run DSO [4] on a continuous sequence of images; being a direct method for visual odometry, DSO is more sensitive to RS distortion compared to the feature-based approaches (*e.g.*, ORB-SLAM [15]). Fig. 4 shows the qualitative results for a particular sequence (id #2) in the TUM dataset; as the first row illustrates, DSO totally fails on the RS images with an EPE of **5.646** pixels. The scene on the second row is reconstructed by DSO on our recovered GS_1 images, which clearly shows the accurate room layout; the EPE for this case is zero by definition. Moreover, we run DSO 100 times and calculate the average absolute trajectory error (ATE). For the RS images, the ATE is **0.273** meter, while it reduces to **0.051** meter for the GS_1 images. These qualitative and quantitative results validate our data generation process and justify the use of EPE as an evaluation metric.

4.2 Improvement by Eliminating Motion Assumption

Next, we demonstrate that the RS distortion can be better corrected by gradually relaxing the camera motion assumptions, *i.e.*, by using an increasing number of pose anchors to essentially accommodate the representation of more complex camera motions. In this section, we use the generated ground truth (GS_1) data to prove this claim in theory.

First, we evaluate the EPE scores for an increasing number of anchors. We stop at 256 anchors as our image height is 256. As reported in Table 1, the EPE scores decrease with more anchors and seem to converge for $N = 8$, which can be due to the fact that we have only 3.6 ground truth poses for each image in the TUM rolling shutter dataset. On the other hand, the converged EPE score is larger than zero; a potential reason is that the cubic spline is defined globally with all ground truth poses during data generation, while it is defined locally with anchors in the current image making the interpolated pose non-identical. Nevertheless, these results show that RS distortion can be better corrected with increasingly more anchors. Moreover, the EPE for $Anchor = 1$ is relatively large, which indicates that the RS image generation with the constant velocity assumption (as in [30]) cannot fully synthesize real RS distortion.

For further validation, we run DSO 100 times on images recovered with one and eight anchors. As demonstrated in Table 1, the ATE slightly decreases when

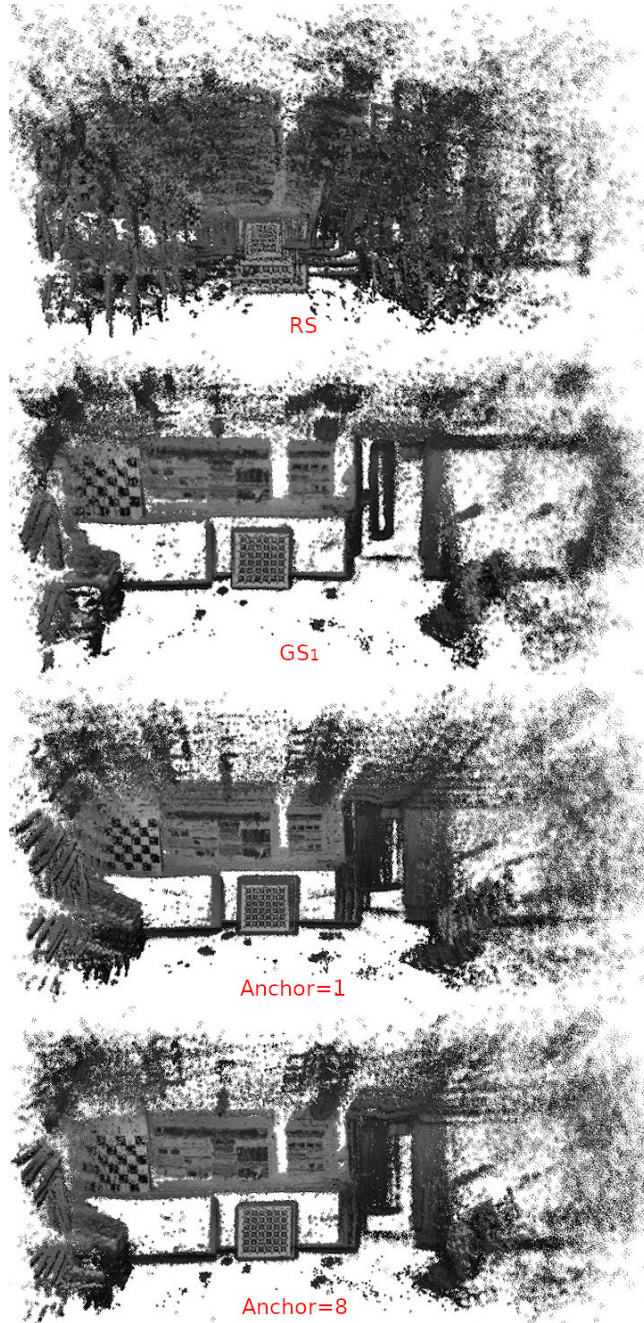


Figure 4: Top to bottom: scenes reconstructed by DSO on RS images, on GS_1 images, with 1 anchor, and with 8 anchors.

more anchors are used. Moreover, as Fig. 4 illustrates, the scene reconstructed with eight anchors (bottom row) is considerably more accurate than using a single anchor (third row), and comparable to the one reconstructed with GS_1 images (second row).

4.3 Network Experiments

Over the 10 sequences of the dataset, the camera motions and the views are diverse by sequence. For instance, the camera rotates in place in sequence #7; intensive acceleration is applied in sequence #9; the camera looks at a single view in sequence #1. To ensure that our network is able to learn from a diverse set of examples and to avoid overfitting, we first randomly permute all frames, then take 80% for training, 10% for validation, and 10% for testing.

We follow the training setup used in the VelocityNet [30] for a fair comparison. First the pre-trained weights of ResNet-34 from ImageNet classification are loaded and the weight of translation in the loss function is set to 0.3. Then the training is invoked with a batch size of 40. Nevertheless, there are three major differences: (i) our implementation is based on Keras [7], (ii) image size is 320×256 , and (iii) the learning rate of Adam optimizer [13] is exponentially decayed (from 10^{-4} to 10^{-5}). Our training platform is an Nvidia™ GTX Titan V GPU with 12GB memory. Since the AnchorNet degenerates to VelocityNet when $N = 1$, we refer to its analogous results while using a single anchor.

Table 2: The ratio of images whose RS distortion get reduced and EPE with an increasing number of anchors. The ‘Ratio’ and ‘EPE’ are based on the predicted anchors and predicted depth map; the ‘Ratio*’ and ‘EPE*’ are based on the predicted anchors and ground truth depth map. EPE of testing RS images is 4.731 pixels.

Anchor	1	2	4	8	16	32	64	128	256
Ratio (%)	93.8	93.7	93.8	93.7	93.3	93.9	94.7	93.3	94.5
EPE (px)	1.636	1.658	1.556	1.465	1.464	1.407	1.348	1.360	1.223
Ratio* (%)	93.9	93.9	93.9	93.9	93.1	93.9	94.9	93.5	94.7
EPE* (px)	1.614	1.637	1.537	1.446	1.445	1.388	1.330	1.345	1.206

Table 2 reports the performance comparisons on test data. The *Ratio* represents the percentage of testing images whose RS distortion (measured by EPE) gets reduced. Regardless of the number of anchors, the network performs well with a *Ratio* larger than 93%. Besides, there is a clear trend for EPE that it decreases with an increasing number of anchors. The cumulative distribution function curves in Fig. 5a further validates the statements above. To isolate the DepthNet error, we also report the results with AnchorNet and ground truth depth map at the bottom half of Table 2. These results validate that the performance gain is solely because of using more anchors. One note is that unlike Table 1 where EPE converges for $N = 8$ anchors, the EPE in Table 2 keeps

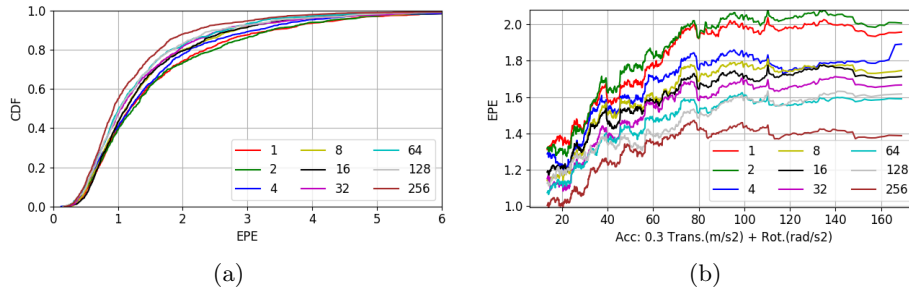


Figure 5: (a): The cumulative distribution function (CDF) curves of EPEs with different number of anchors. (b): EPEs against acceleration with different anchors. The EPEs are sorted by acceleration and averaged with nearby 200 samples. The acceleration is calculated with the same weight on the translation as [30].

decreasing with more anchors. The most likely reason is that the cubic spline with more anchors is more robust to outliers.

Moreover, in Fig. 5b, we plot the EPEs against motion acceleration. As it shows, not only the overall EPE decreases with more anchors, but also the error is less sensitive to the acceleration. Thus, we conclude that the network learns better for RS correction with relaxed motion assumptions ensured by using more anchors.

Table 3: The final reprojection errors of COLMAP on RS images, on GS_1 images, with a single anchor, and with $N = 256$ anchors.

Images	RS	$N = 1$	$N = 256$	GS_1
Error (px)	1.083	0.871	0.810	0.816

Furthermore, to show that other vision-based algorithms can benefit from this, we run COLMAP [21], a structure-from-motion application, on the predicted GS images. Table 3 shows the final reprojection errors; as the results suggest, the error on RS images is clearly larger than both the ground truth GS_1 images and the predicted GS images. We can also see the improvement of having more anchors. Additionally, Fig. 6 shows the visual results of COLMAP on the predicted GS images with 256 anchors.

Lastly, we present some qualitative results of end-to-end RS correction by the proposed system in Fig. 7. It shows that the predicted GS images look very close to the ground truth images, as most of the visible RS distortions are removed.

4.4 Ablation Experiments

Finally, we analyze the generalizability and design choices for AnchorNet with two sets of ablation studies: (i) with a much deeper ResNet-50 backbone, and (ii) with a VGG-16 backbone pre-trained on ImageNet. As Table 4 indicates, we observe the same trend in RS correction performance irrespective of the choice of backbone feature extractors. These results strongly support our idea and validate the effectiveness of using pose anchors to relax camera motion assumptions for learning RS correction.

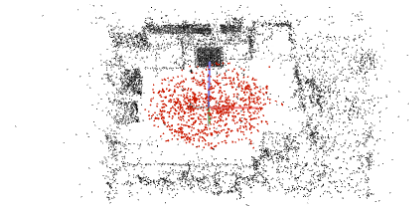


Figure 6: The results of COLMAP reconstruction on rectified images similar to those shown in Fig. 7, as predicted by our network with $N = 256$ anchors. Here, the red cones represent camera positions.

Table 4: EPEs with different choices of base networks: ResNet-34, ResNet-50, and VGG-16.

Anchor	1	2	4	8	16	32	64	128	256
ResNet34	1.636	1.658	1.556	1.465	1.464	1.407	1.348	1.360	1.223
ResNet50	1.733	1.770	1.703	1.675	1.507	1.496	1.429	1.365	1.327
VGG16	1.473	1.447	1.515	1.534	1.476	1.379	1.354	1.336	1.328

Interestingly, we notice that for $N = 1$, *i.e.*, the VelocityNet configuration, performs much better with a VGG-16 backbone. However, we observe that ResNet-34 provides slightly better and more consistent results with an increasing number of anchors, particularly for $N \geq 8$. Moreover, the additional residual layers in ResNet-50 do not provide any performance boosts in the learning. Hence, we remain with ResNet-34 as the default feature extractor of the proposed AnchorNet architecture (see Fig. 3).

5 Conclusions

We propose a novel approach to train a neural network for single-frame rolling shutter correction without any assumptions on camera motion. We propose the AnchorNet architecture which eliminates the camera motion assumption by using a variable number of *pose anchors* to robustly correct rolling shutter distortions. Rather than synthesizing rolling shutter images with certain motion assumption, we generate real images from [22] to train the proposed deep neural network. Our experiments validate the improved accuracy and robustness in rolling shutter correction and downstream vision algorithms by using the proposed approach. For future work, we aim to extend AnchorNet for use in diverse environments, which would require the design of our own data acquisition device. We also intend to tune the proposed method for real-time performance. This would allow the use of the proposed approach for vision-based robot localiza-

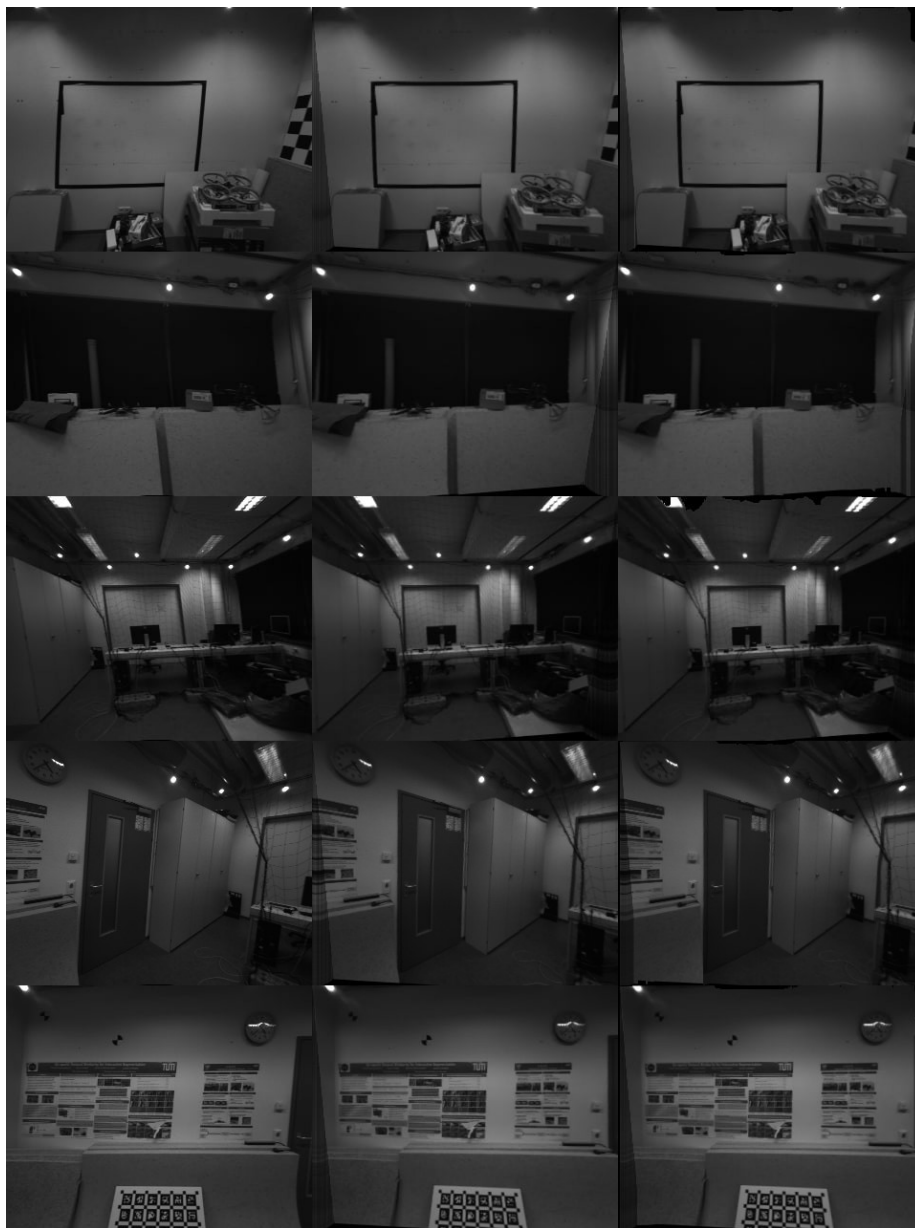


Figure 7: Samples of predicted GS images by the network with 256 anchors. The first column is the input RS images; the second column is the predicted GS images; the third column is the ground truth GS₁ images.

tion and odometry purposes in challenging domains (*e.g.*, aerial and underwater inspections) while using inexpensive and ubiquitous rolling shutter cameras.

Acknowledgement

We thank Slinko *et al.* [24] for sharing the weights of PWC-Net on grayscale images with us. We are also thankful to NvidiaTM for their donation of GPUs to support our work.

References

- [1] Cenek Albl, Zuzana Kukelova, and Tomas Pajdla. R6P-Rolling Shutter Absolute Camera Pose. In *Proceedings of the IEEE Conference on Computer Vision and Pattern Recognition*, pages 2292–2300, 2015.
- [2] Weifeng Chen, Zhao Fu, Dawei Yang, and Jia Deng. Single-Image Depth Perception in the Wild. In *Advances in Neural Information Processing Systems*, pages 730–738, 2016.
- [3] Arun CS Kumar, Suchendra M Bhandarkar, and Mukta Prasad. DepthNet: A Recurrent Neural Network Architecture for Monocular Depth Prediction. In *Proceedings of the IEEE Conference on Computer Vision and Pattern Recognition Workshops*, pages 283–291, 2018.
- [4] Jakob Engel, Vladlen Koltun, and Daniel Cremers. Direct Sparse Odometry. *IEEE Transactions on Pattern Analysis and Machine Intelligence*, 40(3):611–625, 2017.
- [5] Andreas Geiger, Philip Lenz, Christoph Stiller, and Raquel Urtasun. Vision Meets Robotics: The KITTI Dataset. *The International Journal of Robotics Research*, 32(11):1231–1237, 2013.
- [6] Ian Goodfellow, Yoshua Bengio, and Aaron Courville. *Deep Learning*. MIT press, 2016.
- [7] Antonio Gulli and Sujit Pal. *Deep Learning with Keras*. Packt Publishing Ltd, 2017.
- [8] Chao X Guo, Dimitrios G Kottas, Ryan DuToit, Ahmed Ahmed, Ruipeng Li, and Stergios I Roumeliotis. Efficient Visual-Inertial Navigation using a Rolling-Shutter Camera with Inaccurate Timestamps. In *Robotics: Science and Systems*. Citeseer, 2014.
- [9] Kaiming He, Xiangyu Zhang, Shaoqing Ren, and Jian Sun. Deep Residual Learning for Image Recognition. In *IEEE Conference on Computer Vision and Pattern Recognition (CVPR)*, pages 770–778. IEEE, 2016.

- [10] Brian Heflin, Walter Scheirer, and Terrence E Boulton. Correcting Rolling-Shutter Distortion of CMOS Sensors using Facial Feature Detection. In *2010 Fourth IEEE International Conference on Biometrics: Theory, Applications and Systems (BTAS)*, pages 1–6. IEEE, 2010.
- [11] Heiko Hirschmuller. Stereo Processing by Semi-Global Matching and Mutual Information. *IEEE Transactions on Pattern Analysis and Machine Intelligence*, 30(2):328–341, 2007.
- [12] Sergey Ioffe and Christian Szegedy. Batch Normalization: Accelerating Deep Network Training by Reducing Internal Covariate Shift. *CoRR*, abs/1502.03167, 2015.
- [13] Diederik P Kingma and Jimmy Ba. Adam: A Method for Stochastic Optimization. *arXiv preprint arXiv:1412.6980*, 2014.
- [14] Nikolaus Mayer, Eddy Ilg, Philip Hausser, Philipp Fischer, Daniel Cremers, Alexey Dosovitskiy, and Thomas Brox. A Large Dataset to Train Convolutional Networks for Disparity, Optical Flow, and Scene Flow Estimation. In *Proceedings of the IEEE Conference on Computer Vision and Pattern Recognition*, pages 4040–4048, 2016.
- [15] Raul Mur-Artal, Jose Maria Martinez Montiel, and Juan D Tardos. ORB-SLAM: a Versatile and Accurate Monocular SLAM System. *IEEE Transactions on Robotics*, 31(5):1147–1163, 2015.
- [16] Vinod Nair and Geoffrey E Hinton. Rectified Linear Units Improve Restricted Boltzmann Machines. In *Proc. of the International Conference on Machine Learning (ICML)*, pages 807–814, 2010.
- [17] Pulak Purkait, Christopher Zach, and Ales Leonardis. Rolling Shutter Correction in Manhattan World. In *Proceedings of the IEEE International Conference on Computer Vision*, pages 882–890, 2017.
- [18] Vijay Rengarajan, Yogesh Balaji, and AN Rajagopalan. Unrolling the Shutter: CNN to Correct Motion Distortions. In *Proceedings of the IEEE Conference on Computer Vision and Pattern Recognition*, pages 2291–2299, 2017.
- [19] Erik Ringaby and Per-Erik Forssén. Efficient Video Rectification and Stabilisation for Cell-phones. *International Journal of Computer Vision*, 96(3):335–352, 2012.
- [20] Isaac Jacob Schoenberg. Contributions to the Problem of Approximation of Equidistant Data by Analytic Functions Part B—On the Problem of Osculatory Interpolation. A Second Class of Analytic Approximation Formulae. *Quarterly of Applied Mathematics*, 4(2):112–141, 1946.

- [21] Johannes Lutz Schönberger and Jan-Michael Frahm. Structure-from-Motion Revisited. In *Conference on Computer Vision and Pattern Recognition (CVPR)*, 2016.
- [22] David Schubert, Nikolaus Demmel, Lukas von Stumberg, Vladyslav Usenko, and Daniel Cremers. Rolling-Shutter Modelling for Direct Visual-Inertial Odometry. *arXiv preprint arXiv:1911.01015*, 2019.
- [23] Karen Simonyan and Andrew Zisserman. Very Deep Convolutional Networks for Large-scale Image Recognition. *arXiv preprint arXiv:1409.1556*, 2014.
- [24] Igor Slinko, Anna Vorontsova, Dmitry Zhukov, Olga Barinova, and Anton Komushin. Training Deep SLAM on Single Frames. *arXiv preprint arXiv:1912.05405*, 2019.
- [25] Deqing Sun, Xiaodong Yang, Ming-Yu Liu, and Jan Kautz. PWC-Net: CNNs for Optical Flow Using Pyramid, Warping, and Cost Volume. In *Proceedings of the IEEE Conference on Computer Vision and Pattern Recognition*, pages 8934–8943, 2018.
- [26] Benjamin Ummenhofer, Huizhong Zhou, Jonas Uhrig, Nikolaus Mayer, Eddy Ilg, Alexey Dosovitskiy, and Thomas Brox. DeMoN: Depth and Motion Network for Learning Monocular Stereo. In *Proceedings of the IEEE Conference on Computer Vision and Pattern Recognition*, pages 5038–5047, 2017.
- [27] Sudheendra Vijayanarasimhan, Susanna Ricco, Cordelia Schmid, Rahul Sukthankar, and Katerina Fragkiadaki. SfM-Net: Learning of Structure and Motion from Video. *arXiv preprint arXiv:1704.07804*, 2017.
- [28] George Vogiatzis and Carlos Hernández. Video-based, Real-Time Multi View Stereo. *Image and Vision Computing*, 29(7):434–441, 2011.
- [29] Bingbing Zhuang, Loong-Fah Cheong, and Gim Hee Lee. Rolling-Shutter-Aware Differential SfM and Image Rectification. In *Proceedings of the IEEE International Conference on Computer Vision*, pages 948–956, 2017.
- [30] Bingbing Zhuang, Quoc-Huy Tran, Pan Ji, Loong-Fah Cheong, and Manmohan Chandraker. Learning Structure-And-Motion-Aware Rolling Shutter Correction. In *Proceedings of the IEEE Conference on Computer Vision and Pattern Recognition*, pages 4551–4560, 2019.